Model-Free Control of Single-Phase Boost AC/DC Converters

Hengguo Zhang, Hongmei Li, Jingkui Mao, Chen Pan, and Zhiyuan Luan

***Abstract*—Conventionally, the benchmark proportional-integral control method is implemented to realize power factor correction and output voltage regulation of single-phase ac/dc converters. However, the performance is deteriorated due to the influence of uncertainties and disturbances, e.g., periodic input voltage and load variation. Concerning this problem, this article proposes a model-free control (MFC) strategy of single-phase ac/dc converters. The MFC principle is revisited and a frequency response analysis is presented for the algebraic estimators of uncertainties and disturbances. Consequently, the closed-loop performance of MFC systems is allowed to be analyzed in frequency domain via classical linear control theory. Based on the theoretical results, the model-free current and voltage control systems are synthesized in detail to achieve control objectives of the converter. Simulation results demonstrate the performance of MFC systems in reference tracking and disturbance rejection. The feasibility and validity of the presented MFC strategy for single-phase boost ac/dc converters is also confirmed experimentally as compared to the benchmark scheme.**

***Index Terms*—Algebraic estimation, double-frequency ripple, model-free control (MFC), power factor correction (PFC), single-phase ac/dc converter.**

I. Introduction

NOWADAYS, single-phase ac/dc converters with power factor correction (PFC) have been widely used in industrial applications. The wireless power transfer system and on-board charger of electric vehicles are typical examples on the front-end PFC [1], [2]. Among various topologies, boost converter operating in continuous conduction mode is the most favorite one in medium-to-high power applications. For single-phase boost ac/dc converters, the input current and output voltage need to be controlled to realize unity power factor operation with a tight output voltage regulation. To this end, dual-loop average current control strategy is adopted. The inner current controller forces the input current to follow its reference which is proportional to the varying input voltage. The outer voltage control system regulates the average output voltage to balance average input and output power of the converter.

In general, input current of the converter is required to track a time-varying reference trajectory while rejecting the effect of input and output voltages. Under these circumstances, line current is usually distorted due to the limited bandwidth of the proportional-integral (PI) current control system. Duty ratio feed-forward (FF) control is proposed [3]. Current phase lead effect caused by input voltage can be alleviated and current distortion is reduced [4]. Considering the periodicity of current distortion, repetitive control is also used for a bridgeless PFC converter [5]. Researches in [6] and [7] focus on the predictive control of PFC converters and optimal duty ratio is obtained including operation mode detection [6]. The concern, however, is the sensitivity of predictive control to unmodeled dynamics and parameter uncertainties of the converter. To address this issue, a predictive current controller including major nonideal terms of the converter and a moving average based one are compared in [7]. Effectiveness of the latter is fully proved in terms of control performance and computational complexity. Besides, sliding mode control has also been applied to PFC converters. In [8], a sliding mode current controller operating at constant switching frequency is designed for an interleaved boost PFC converter, of which the output voltage is governed by an outer PI controller. Loss-free resistor behavior can be imposed on the converter with voltage regulation capability based on adaptive sliding mode control [9]. Furthermore, in [10], a sliding mode surface including current and voltage errors and their integrals can maintain a unity power factor and good dynamic performance simultaneously.

Other than the load variations in voltage control system, one particular issue is the double-line frequency ripple on the dc-side output voltage. It is a byproduct of PFC and it remains a challenge to balance the performance of dynamic response and ac-side current quality of the converter [11]. Typical methods for this problem are to block the ripple voltage preventing it from entering the control loop, among which the notch filter (NF) has been the representative solution. In [12] and [13], an NF tuned at double-line frequency is used to remove the ripple voltage and improve the bandwidth of voltage control system. An improved voltage control method is presented in [14] by using the feedback of internal dynamics of the NF. Enhanced transient performance is obtained as the internal variables of NF share the dynamics of current control system. Though the bandwidth is increased, NFs cause extra dynamics and limit

Manuscript received September 8, 2021; revised December 22, 2021 and March 25, 2022; accepted May 8, 2022. Date of publication May 23, 2022; date of current version June 24, 2022. This work was supported in part by the National Natural Science Foundation of China under Grant 51877064 and in part by the Anhui Provincial Key Research and Development Program Funding under Grant 1804a09020092. Recommended for publication by Associate Editor A. Yazdani. *(Corresponding author: Hongmei Li.)*

The authors are with the School of Electrical Engineering and Automation, Hefei University of Technology, Hefei 230009, China (e-mail: zhhg@mail.hfut.edu.cn; hongmei.li@hfut.edu.cn; maojingkui@126.com; 601739255@qq.com; luan.zhiyuan@foxmail.com).

Color versions of one or more figures in this article are available at https://doi.org/10.1109/TPEL.2022.3176937.

Digital Object Identifier 10.1109/TPEL.2022.3176937

the performance of voltage control systems. A dc estimation method without NF is proposed and a high robustness against load variations of the system is obtained [15]. In [16], effect of the ripple voltage is canceled without adding any filters in the voltage loop by using current-harmonic FF scheme. Since a PI controller with constant gains faces the tradeoff between voltage fluctuation and current distortion, an adaptive and a nonlinear PI voltage control methods are adopted in [17] and [18], respectively. The gains of PI controller are self-tuned according to the voltage error band defined in advance. This adaptive process allows a fast transient voltage dynamic and a low current distortion in steady state.

Since single-phase boost ac/dc converters undergo various disturbances, e.g., inductance variations and load changes, this article investigates the model-free control (MFC) approach to improve current quality and voltage dynamics of the converter. The MFC approach, which was proposed by Fliess and his coworkers, have emerged as a simple and effective solution for robust control of uncertain systems with disturbances [27]. In the context of MFC, an ultralocal model (ULM) is used to approximate the input-output behavior of uncertain systems locally, in which the poorly known part and disturbances are encompassed into a single unknown quantity without explicit distinction between them. Apart from this concept, core part of MFC is the algebraic estimation technique for this unknown quantity, which employs elementary operational calculus and differential algebra. It allows the ULM to be updated online by using the system input and output. Though other methods, e.g., extended state observers (ESOs) [28], have been alternatively used, it behaves in an algebraic and nonasymptotic manner and is robust to initial conditions and noises [29]. In the last decades, it has been utilized for signal processing [30], [31] and state estimation [32]–[34], etc. Under the assumption of ULM and perfect estimation of uncertainties and disturbances, controller synthesis becomes straightforward to obtain a good tracking performance and does not require a good and global modeling process. The MFC approach has been applied in various fields in the last decade, such as in shape memory alloys actuators [19], vehicle control [20], motor drives [21], wind power generation [22], and smart grid [23]. The efficacy of the ULM concept is demonstrated by concrete successful applications and existing examples show that the order of it may always be chosen low, i.e., 1 or 2 [24]–[26].

However, the assumption of perfect disturbance estimation has practical limitations. The dynamics of algebraic estimators (AEs) may cause bounded output errors in case of incomplete elimination of mismatches between the ULM and real plant or even the instability of MFC systems. To the best of our knowledge, closed-loop performance analysis of a MFC system including AE has not been well resolved. To this end, this article presents a frequency domain analysis method for MFC systems with AEs. The main contributions are summarized as follows.

1) A theoretical analysis for the frequency response of AE is presented. It can be characterized by a specially designed low-pass filter. The key design parameter, i.e., the width of sliding time window, can be connected to the filter bandwidth.
2) Consequently, the closed-loop MFC system is revisited in frequency domain to provide an insight of it in reference tracking and disturbance rejection.
3) A holistic MFC strategy is synthesized for current and voltage control systems of a boost PFC converter. Both the abovementioned theoretical analysis and the proposed MFC method of the converter are validated by simulation and experimental results.

II. Model-free Control

A. Overviews

For a system with a single control input and a single output, behavior of the system is assumed to be well approximated and can be expressed with an algebraic differential equation as

$$E(t, y, \dot{y}, \ldots, y^{(n)}, \ldots y^{(a)}, u, \dot{u}, \ldots, u^{(b)}) = 0 \tag{1}$$

where u and y are the system input and output, respectively; E is a poorly known, but derivable function; the superscript $(\cdot)$ denotes the orders of derivative with n, a and b being positive integers. Equation (1) can be dynamically substituted by ULM of the form [27]

$$y^{(n)}(t) = F(t) + \alpha u(t) \tag{2}$$

where α is a nonphysical parameter and it is designed such that both sides of (2) are of the same magnitude. The variable $F(t)$, which is continuously updated, denotes the poorly known part of the system as well as various possible disturbances. Its estimation can be determined by utilizing the input-output behavior of the system, which will be elaborated later.

Considering that the derivative order n in (2) may always be selected quite low, we restrict ourselves for simplicity's sake to the case of $n = 1$ in this article. Closing the loop via intelligent controllers leads to the following control law

$$u(t) = \frac{\dot{y}_{\mathrm{r}}(t) - F(t) + C(t) \otimes e(t)}{\alpha} \tag{3}$$

where $\dot{y}_r(t)$ is the first-order derivative of the output reference $y_r(t)$. $C(t)$ represents the unity impulse response of the tracking controller.'$\otimes$' denotes the conventional convolution operator and $e(t) = y_r(t)$-$y(t)$ is the tracking error.

Usually, $F(t)$ contains uncertain and unmeasurable terms. It cannot be obtained directly, but could be properly estimated via the AE approach. Provided that $F(t)$ is slow-varying and is approximated by a piecewise constant function, the estimation of $F(t)$ can be consequently achieved via the estimation of an unknown constant parameter ψ in a short time interval and (2) can be rewritten as

$$\dot{y}(t) = \psi + \alpha u(t). \tag{4}$$

Applying the Laplace transform of (4) yields

$$sy(s) - y(0) = \frac{\psi}{s} + \alpha u(s) \tag{5}$$

where s and $y(0)$ denotes the Laplace variable and the initial condition of y, respectively.

To eliminate $y(0)$ and subsequently assure that each term in (5) is integrated once in time domain for smoothing the noise,

one can apply the linear differential operator of the form

$$\Pi = \frac{1}{s^2}\frac{\mathrm{d}}{\mathrm{d}s} \tag{6}$$

to both sides of (5). It results in

$$-\frac{\psi}{s^4} = \frac{1}{s^2}y(s) + \frac{1}{s}\frac{\mathrm{d}}{\mathrm{d}s}y(s) - \frac{\alpha}{s^2}\frac{\mathrm{d}}{\mathrm{d}s}u(s) \tag{7}$$

in which the positive powers of s are avoided.

Consequently, the unknown constant ψ can be obtained by using the inverse Laplace transform and Cauchy formula. In a sliding time window with fixed width T, it is expressed as

$$\psi = -\frac{6}{T^3}\int_0^T \left[(T-2\tau')y(\tau') + \alpha(T-\tau')\tau' u(\tau')\right]\mathrm{d}\tau' \tag{8}$$

where $\tau'$is the integral variable in the sliding time window.

In practice, (8) can be digitally realized via trapezoidal rule and the instant T corresponds to the current control period. It results in the real-time estimation via a finite impulse response (FIR) filter. Thus, the AE for uncertainties and disturbances is causal and stable. Compared to asymptotic estimation methods, AE allows one to get the estimation result in an arbitrary finite time and is robust to unknown initial conditions in a noisy environment.

Once the estimation process is completed, $F(t)$ in (3) is substituted by its estimation $F_e(t) = \psi$. Moreover, the derivative of output reference in (3) can be omitted in order to simplify the controller design. Therefore, the control law in (3) can be rearranged as

$$u(t) = \frac{-F_e(t) + C(t) \otimes e(t)}{\alpha}. \tag{9}$$

Combining (9) and the corresponding ULM in (2), one can obtain the output response as

$$\dot{y}(t) = C(t) \otimes e(t) + F(t) - F_e(t). \tag{10}$$

Given that a good estimation of the unknown quantity $F(t)$ is obtained so that the estimation error satisfies $F(t)$-$F_e(t) = 0$, output of the system is exclusively determined by the tracking controller. The closed-loop transfer function of the system is obtained as

$$\frac{y(s)}{y_r(s)} = \frac{C(s)}{s + C(s)} \tag{11}$$

where $y_r(s)$ and $C(s)$ are the counterparts of $y_r(t)$ and $C(t)$ in complex domain, respectively. If an intelligent proportional controller, i.e., $C(s) = k_p$, is adopted, it leads to a closed-loop system with a time constant related to the coefficient k_p.

B. Frequency Response of AE

In practical control systems, the uncertain part of the system and external disturbances are characterized as nonlinear and time-varying, e.g., the periodic disturbance in grid-connected power converters [35]. The complex disturbance is difficult to be estimated accurately. Besides, the AE method assumes the approximation of uncertainties and disturbances in a piecewise constant manner, which may lead to estimation errors. In these circumstances, the accuracy of AE needs to be evaluated as it will affect the control performance as shown in (10). To this end, this article presents a frequency domain analysis method for the closed-loop MFC system. It turns out that the AE can be characterized by a specially designed smoothing filter.

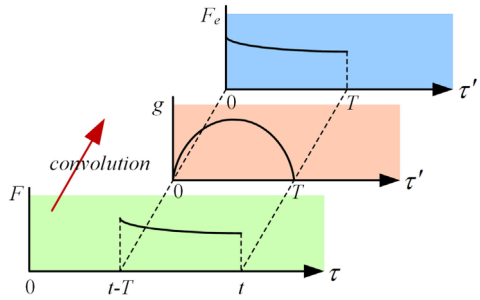

Fig. 1. Illustration of the estimation process of AE in sliding time windows.

Consider again the estimation process of AE for $F(t)$ and the corresponding ULM, (5) is rewritten as

$$\frac{\psi}{s} = F(s) \tag{12}$$

where $F(s)$ is the counterpart of $F(t)$ in complex domain.

By applying the same linear differential operator (6) to both sides of (12), it yields

$$-\frac{\psi}{s^4} = \frac{1}{s^2}\frac{\mathrm{d}}{\mathrm{d}s}F(s). \tag{13}$$

Hence, ψ is estimated in time domain with respect to $F(t)$ as

$$\psi = \frac{6}{T^3}\int_0^T (T-\tau')\tau' F(\tau')\mathrm{d}\tau'. \tag{14}$$

To show the integration process mathematically in a sliding time window, one can move the time origin from 0 to t-T and thus obtain the estimation in a time interval [t-T, t]. As shown in Fig. 1, these sliding time windows allow the estimation of $F(t)$ in real-time. Substituting the transformation of time

$$\tau = \tau' + t - T \tag{15}$$

into (14) leads to

$$\psi = \frac{6}{T^3}\int_{t-T}^{t} (t-\tau)(\tau - (t-T))F(\tau)d\tau \tag{16}$$

where τ is the integral variable.

Define $g(t) = \frac{6}{T^3}(T-t)t$ with $t \in [0, T]$, the estimation of $F(t)$ is obtained in a convolution integration form shown as

$$F_e(t) = g(t) \otimes F(t) = \int_{t-T}^{t} g(t-\tau)F(\tau)d\tau. \tag{17}$$

According to the properties of convolution operation, (17) can be represented in complex domain as

$$F_e(s) = G(s)F(s) \tag{18}$$

where $F_e(s)$ and $G(s)$ are the counterpart of $F_e(t)$ and $g(t)$ in complex domain, respectively.

It can be seen from (18) that the AE method of continuous disturbance signal is equivalent to approximating it via a filter $G(s)$, which is designed with a unity impulse response of $g(t)$.

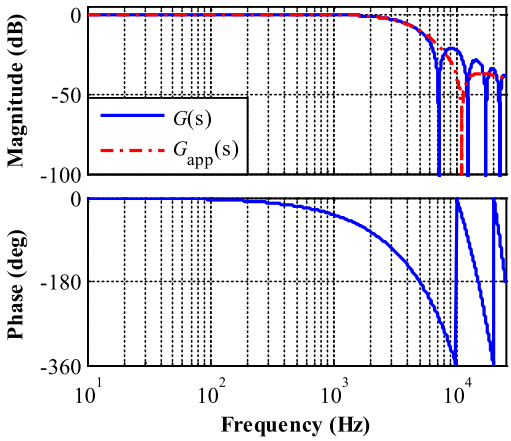

Fig. 2. Frequency response of the AE ($T = 200\ \mu$s).

Hence, the properties of AE of uncertainties and disturbances are determined by this special filter. With the definition of $g(t)$, the expression of $G(s)$ can be obtained via Laplace transform shown as

$$G(s) = \frac{6}{s^2T^2}\left[(e^{-sT}+1) + \frac{2}{sT}(e^{-sT}-1)\right]. \tag{19}$$

Substituting $s = iw$ into (19) and taking the Euler identity into consideration, it yields

$$G(iw) = e^{-iwT/2}\frac{12}{w^2T^2}\left[\frac{2}{wT}\sin wT/2 - \cos wT/2\right] \tag{20}$$

where w and i denote the angular frequency in rad/s and the imaginary unit, respectively.

The frequency response of *AE* is consequently derived as follows:

$$\begin{cases} |G(iw)| = \frac{12}{w^2T^2}\left(\frac{2}{wT}\sin wT/2 - \cos wT/2\right) \\ \varphi(w) = -wT/2 \end{cases}. \tag{21}$$

Fig. 2 shows the magnitude and phase of $G(s)$ with respect to frequency in Hz. It can be observed from Fig. 2 that the filter exhibits a flat low-passing property with a linear phase shift. The magnitude attenuation is maintained close to 0 dB in the passing band of the filter, which means that the original disturbance signal is estimated with negligible amplification or attenuation. Moreover, the phase delay of the filter is almost maintained at 0° in the low frequency range (e.g., lower than 100 Hz). These are preferable characteristics for estimating the disturbance signal. Based on (21), there is

$$\lim_{w\to 0}|G(iw)| = 1. \tag{22}$$

Considering the complexity of (19), proper simplification is helpful to characterize the filter properties. By applying the second-order Pade approximation, (19) is simplified as

$$G_{\text{app}}(s) = e^{-sT/2}\frac{12s^2T^2 + 48^2}{s^4T^4 - 48s^2T^2 + 48^2}. \tag{23}$$

Fig. 2 also presents the frequency response of (23). It is shown that (19) and (23) exhibit identical phase property with almost the same magnitude attenuation in the passing band of the filter. Thus, the properties of $G(s)$ can be partly depicted by (23). Based on this, one can obtain the -3 dB bandwidth of $G(s)$ in radians from (23) as follows:

$$w_{\text{AE}} = \frac{1}{T}\sqrt{12.34} \tag{24}$$

in which the bandwidth is inverse proportional to the width of the sliding time window. Based on this fact, the parameter T can be designed according to the desired frequency response of $G(s)$. Moreover, it can be inferred that a short time window is preferable for uncertainty and disturbance estimation with unity gain and reduced phase shift. However, it sacrifices the capability of noise rejection and vice versa.

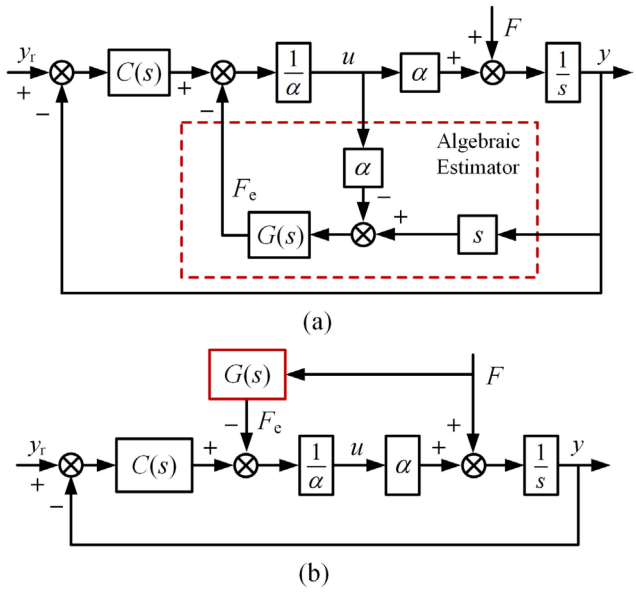

Fig. 3. Block diagram of the MFC system. (a) Overall structure. (b) Simplified equivalent.

C. Frequency Domain Analysis of MFC Systems

To realize the closed-loop analysis of a MFC system, the ULM is presented in complex domain without concerning the initial conditions as

$$sy(s) = F(s) + \alpha u(s). \tag{25}$$

By combining the control law (9), the estimation of $F(t)$ (18) and the ULM (25), one can obtain the MFC system as shown in Fig. 3. The model-free controller is constituted by an AE for the estimation of uncertainties and disturbances and a tracking controller $C(s)$ for tracking error correction. It is shown that the AE is constructed by utilizing the ULM with a smoothing filter $G(s)$. Substituting (18) and (25) into (9) leads to the equivalent model-free controller

$$\alpha u(s) = \frac{C(s)}{1-G(s)}e(s) - \frac{G(s)}{1-G(s)}sy(s) \tag{26}$$

in which the term $1/(1-G(s))$ makes the model-free controller act as an integrator because of the low-passing property of $G(s)$.

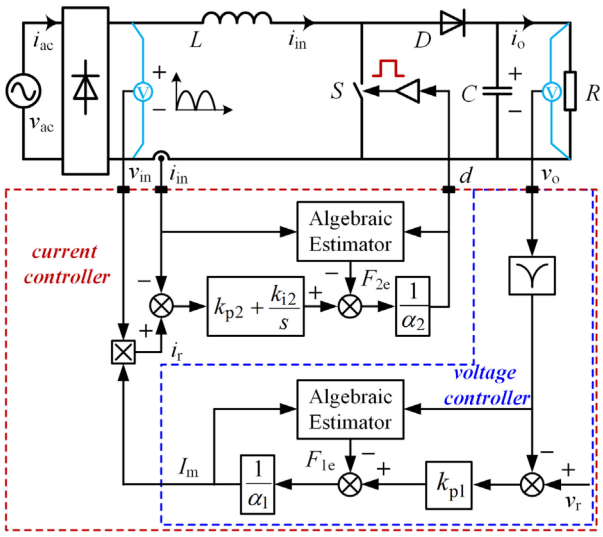

Fig. 4. Schematic diagram of the single-phase boost ac/dc converter with the proposed MFC system.

This coincides with the connections between classic PI and the intelligent controllers as shown in [27]. The integral action can be explained at $s = 0$ as

$$\lim_{s=iw\to 0} \frac{1}{1-G(s)} = \infty. \tag{27}$$

Fig. 3(b) shows the equivalent block diagram of MFC system. By defining $P_n(s) = 1/s$ and substituting (9) and (18) into (25), one can obtain the output of closed-loop system

$$y(s) = \frac{\mathrm{LP}(s)}{1+\mathrm{LP}(s)} y_r(s) + \frac{P_n(s)}{1+\mathrm{LP}(s)} \left[1 - G(s)\right] F(s) \tag{28}$$

where $\mathrm{LP}(s) = P_n(s)C(s)$ denotes the loop gain. From (28), it is evident that the tracking performance and the stability of the closed-loop system are determined by the loop gain. Therefore, the design of $C(s)$ should lead to a stable system with adequate stability margins and reference tracking performance. The AE of uncertainties and disturbances behaves like filtering the real unknown signal and then feeding it back to the loop to cancel out its effects. As shown in (28), the unknown signal $F(t)$ is blocked by 1-$G(s)$. Ideally, system output is only determined by $C(s)$ in case $G(s) = 1$ is always satisfied.

III. Model-Free Control of Boost Ac/Dc Converter

An MFC method is proposed in this article to perform PFC and dc-side voltage regulation of the boost ac/dc converter. Fig. 4 shows the boost converter topology along with its controllers. In the proposed method, the converter is considered as single-input and single-output voltage and current systems in a cascaded manner, which are governed by independent model-free controllers, respectively. The average output voltage is regulated by an outer voltage controller to achieve the power balance between the ac and dc sides of the converter. Meanwhile, an inner current controller governs the input current so that it can accurately track its reference, which is proportional to the rectified input voltage. In this section, the design process is presented and the two controllers are designed independently because of the large bandwidth difference and consequently the decoupling of the two control systems.

A. System Modeling

As presented in Fig. 4, the ac input voltage v_{ac} is rectified via a diode bridge followed by a boost converter. The rectified input voltage of the boost converter is expressed as

$$v_{in} = V_m \left|\sin(wt)\right| \tag{29}$$

where V_m and w are the amplitude and angular frequency of the ac input voltage, respectively.

The state equations of the boost converter are given by [9]

$$\begin{cases} L\frac{di_{in}}{dt} = v_{in} - (1-d)v_o \\ C\frac{dv_o}{dt} = (1-d)i_{in} - i_o \end{cases} \tag{30}$$

where i_{in} and v_o are the input current and output voltage of the converter, respectively. i_o represents the load current. d is the duty ratio of the power switch. L and C denote the inductance and the dc-side capacitance, respectively.

For the convenience of controller design, the current equation in (30) can be reformulated as

$$\begin{cases} \frac{di_{in}}{dt} = \alpha_2 d + F_2 \\ \alpha_2 = \frac{v_o}{L}, F_2 = \frac{v_{in}-v_o}{L} \end{cases} \tag{31}$$

where α_2 denotes the control gain from the duty ratio to the input current. F_2 represents the disturbance mainly caused by the input and output voltage in the current control system.

When the current control system is well regulated, the voltage gain of the boost converter is

$$\frac{v_o}{v_{in}} = \frac{1}{1-d}. \tag{32}$$

Combining (32) and the voltage equation in (30) yields

$$C\frac{dv_o}{dt} = \frac{v_{in}}{v_o} i_{in} - i_o. \tag{33}$$

B. Design of Current Control System

In the current control system, duty ratio and input current are defined as the input and output of the system, respectively. And the input current is regulated to follow the rectified input voltage waveform. To achieve the function of PFC, reference value of the input current is given by

$$i_r = I_m \left|\sin(wt)\right| \tag{34}$$

where I_m denotes the magnitude of reference input current. As will be shown later, I_m is generated by the voltage controller to balance the average input and output power of the converter.

The block diagram of the current control system is shown in Fig. 5. A model-free PI controller is designed to perform the current tracking with low harmonic distortion. The proposed current controller is formulated as

$$d = \frac{-F_{2e} + k_{p2}e_2 + k_{i2}\int_0^t e_2 dt}{\alpha_2} \tag{35}$$

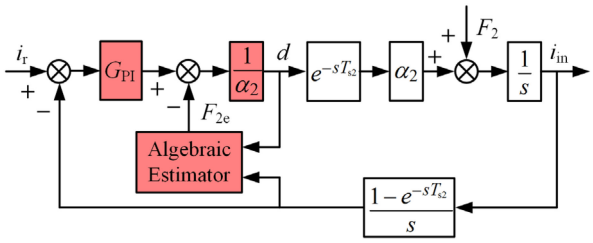

Fig. 5. Block diagram of the model-free current control system.

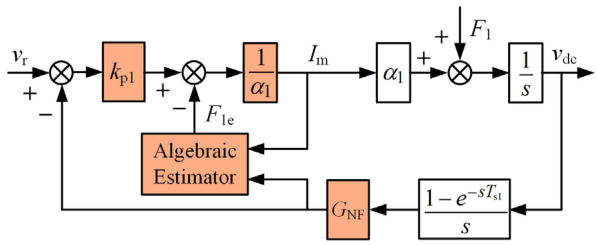

Fig. 6. Block diagram of the simplified model-free voltage control system.

where F_{2e} is the estimation of F_2 by utilizing the AE method. k_{p2} and k_{i2} are the coefficients of the PI controller, respectively. $e_2 = i_r$-i_{in} is the current tracking error.

When F_2 is estimated and compensated, the system model depicted by (31) is equivalent to an integrator. The transfer function from duty ratio to input current is

$$G_{p2}(s) = \frac{i_{in}(s)}{d(s)} = \frac{\alpha_2}{s}. \tag{36}$$

According to the theoretical analysis of an MFC system, the PI controller in (35) should lead to a stable current control system. Time delay caused by the computation time and pulsewidth modulator (PWM) is thus taken into consideration. And the latter is characterized by a zero-order holder (ZOH) [5]. The discrete time version of (36) is given by

$$G_{p2}(z) = \frac{i_{in}(z)}{d(z)} = \alpha_2 \frac{T_{s2}}{z(z-1)} \tag{37}$$

where T_{s2} is the sampling period of the current control system.

To facilitate the implementation of the controller in digital control system, the integral in (35) is discretized by using the trapezoidal integration method. Thus, the transfer function of PI controller in z-domain has the form

$$G_{PI}(z) = k_{p2} + k_{i2}\frac{T_{s2}}{2}\frac{z+1}{z-1}. \tag{38}$$

Combining (37) and (38) yields the loop gain of the current control system

$$LP_2(z) = \alpha_2^{-1} G_{PI}(z) G_{p2}(z) \tag{39}$$

in which the coefficients of PI controller are selected to ensure a current tracking performance with adequate stability margins.

C. Design of Voltage Control System

When designing the voltage control system, it is supposed that the dynamic of current control system is fast enough so that a perfect current tracking is performed. Therefore, the input current of the converter satisfies $i_{in} = i_r$ as shown in (34). By substituting it into (33), the equation describing the voltage control system can be rearranged as

$$\dot{v}_o = \frac{V_m I_m}{2C v_o}(1 - \cos 2wt) - \frac{i_o}{C} \tag{40}$$

in which the rectified input voltage is also considered. From the control point of view, the voltage control system (40) is time-varying. It is not convenient to implement the controller design. More importantly, by solving v_o via (40), it can be concluded that the output voltage contains a ripple component at the double-line frequency in addition to the dc counterpart. If the ripple voltage enters into the control loop via feedback operation, reference of input current will be distorted resulting in a phase shift and additional harmonic components in the grid current [11].

To solve the abovementioned problems, an averaged model is used to describe the output voltage dynamics and design the voltage controller. To this end, (40) is averaged over half of a line cycle [12]. The resulted average model is linear and time invariant and has the form of

$$\dot{v}_{dc} = \frac{V_m}{2C v_{dc}} I_m - \frac{i_o}{C} \tag{41}$$

where v_{dc} is the average output voltage of the converter.

Subsequently, (41) is rearranged as

$$\begin{cases} \dot{v}_{dc} = \alpha_1 I_m + F_1 \\ \alpha_1 = \frac{V_m}{2C v_{dc}}, F_1 = -\frac{i_o}{C} \end{cases} \tag{42}$$

in which the amplitude of reference input current and average output voltage are defined as input and output variables of the system, respectively. F_1 denotes uncertainties and disturbances mainly caused by load variations in the voltage control system. α_1 is the gain from input current amplitude to average output voltage.

The simplified average model of voltage control system is depicted in Fig. 6. The system transfer function is reduced to an integrator when the disturbance F_1 is accurately estimated and cancelled out. Considering the integral effects of model-free controller, a proportional controller is adequate to ensure a perfect tracking of the voltage reference without steady-state tracking error. Thus, the average output voltage is stabilized to its reference v_r via a model-free voltage controller, which is designed of the form

$$I_m = \frac{-F_{1e} + k_{p1} e_1}{\alpha_1} \tag{43}$$

where F_{1e} is the estimation of F_1 by utilizing the AE method. k_{p1} is the coefficient of proportional controller, and $e_1 = v_r - v_{dc}$ is the voltage tracking error.

Because of the ripple component as mentioned previously, the output voltage cannot be used as feedback signals directly. In this article, an FIR NF is employed to remove this ripple voltage in the sampled signal before it enters into the control system. The NF is centered at the double-line frequency and has a transfer

TABLE I
SYSTEM PARAMETERS

System parameter	Value
Input ac voltage v_{ac}	110 Vrms, 50 Hz
Rated Output Power	1000 W
Reference Output Voltage v_r	300 V
Inductance L	486 μH
Capacitance C	990 μF
Switching Frequency f_s	50 kHz
Sampling Period T_{s1}	2.5 ms
Sampling Period T_{s2}	20 μs

function of

$$G_{\mathrm{NF}}(z) = 0.5(1 + z^{-2}) \tag{44}$$

in which the sampling frequency is determined as 400 Hz.

In the digital voltage control system, the sampling process is described by a ZOH as shown in Fig. 6. The discrete time transfer function of (42) is thus given by

$$G_{p1}(z) = \frac{v_{\mathrm{dc}}(z)}{I_m(z)} = \alpha_1 \frac{T_{s1}}{z-1} \tag{45}$$

where T_{s1} is the sampling period of the outer voltage control system.

Consequently, the loop gain of voltage control system can be obtained in discrete time domain and is given by

$$\mathrm{LP}_1(z) = \alpha_1^{-1} k_{p1} G_{\mathrm{NF}}(z) G_{p1}(z). \tag{46}$$

IV. PERFORMANCE EVALUATION

In this section, both simulation verification and experiment tests are carried out to confirm the validity of proposed control method. Specifications of the boost ac/dc converter are given in Table I.

The current and voltage control systems are implemented with different sampling periods, which of the former is 20 μs. And that of the latter is 2.5 ms to comply with the requirement of the NF. To obtain a stable voltage control system, the proportional coefficient k_{p1} is set as 131.5 which results in a positive phase margin of 63° at the crossover frequency of 20 Hz. Fig. 7 shows the open-loop bode plot of voltage control system according to the loop gain presented by (46). For the sake of comparison, two sets of controller parameters for the proposed current control system are designed, respectively. The first set of parameters, named MFCC-I, are designed with $k_{p2} = 18\,200$ and $k_{i2} = 7.8\mathrm{e}7$. And that of the second group, i.e., MFCC-II, are determined to be $k_{p1} = 23000$ and $k_{i1} = 0$, which turns the current tracking controller into a proportional one. Based on (39), one can obtain the characteristics in frequency domain of the current control system as plotted in Fig. 8. It can be seen that the current control system is stable with both groups of controller parameters. System with MFCC-I has a positive phase margin of 45° at the crossover frequency of 3.0 kHz, while that of the system with MFCC-II is 50° at the crossover frequency of 3.7 kHz. Table II gives the controller parameters of the system. As discussed earlier, adequate time windows are needed for both AEs. According to previous sections, the length of the time window is selected to be ten times the sampling period in each control system.

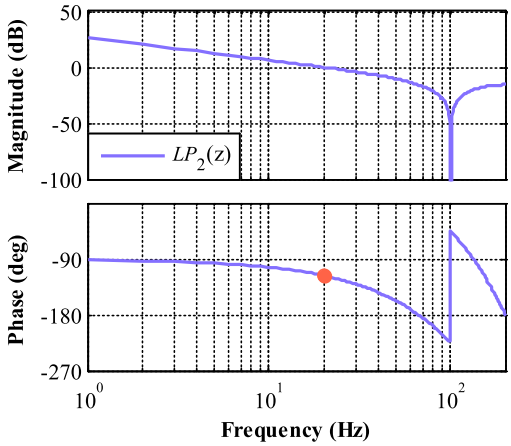

Fig. 7. Open-loop bode plot of the voltage control system.

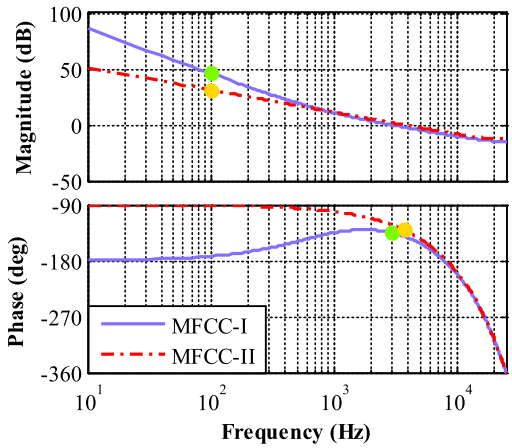

Fig. 8. Open-loop bode plot of the current control system.

TABLE II
CONTROLLER PARAMETERS

The Proposed Control Scheme	
Voltage Controller k_{p1}	131.5
Current Controller MFCC-I k_{p2}	18200
Current Controller MFCC-I k_{i2}	7.8e7
Current Controller MFCC-II k_{p2}	23000
Current Controller MFCC-II k_{i2}	0
The PI Control Scheme	
Current Controller k_{pi}	0.02960
Current Controller k_{ii}	128.1
Voltage Controller k_{pv}	0.4902
Voltage Controller k_{iv}	14.25

A. Simulation Results

To test the proposed MFC method, operation of the single-phase boost ac/dc converter is initially simulated using MATLAB/Simulink software. Converter and controller model parameters are set up according to Tables I and II. Fig. 9 shows the

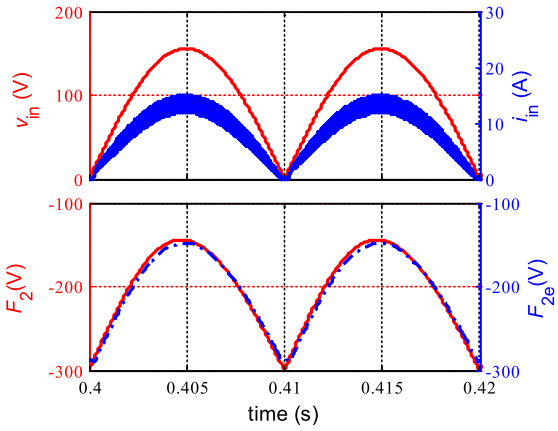

Fig. 9. Simulation results. Steady-state performance of the current control system with MFCC-II when the converter is operated at rated output power.

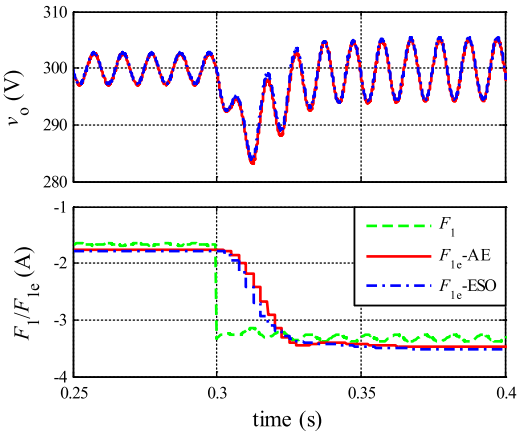

Fig. 10. Simulation results. Transient performance in load step-up from 500 to 1000 W of the voltage control system.

steady-state input current waveform, which follows the rectified input voltage with good accuracy, at rated output power of the converter. The bottom subplot in Fig. 9 presents the disturbance F_2 and its estimation of current control system. Compared to (31), the presented results are multiplied by the inductance L in Table I so that they have the same dimension relation with input and output voltages. As shown in Fig. 2, the AE performs well with negligible phase shift for the disturbance at 100 Hz and this is confirmed by the estimation results of the periodic disturbance in current control system. Consequently, a good tracking performance of input current is achieved with low distortions.

Dynamic response of the converter is also simulated under load power variations. Fig. 10 shows the output voltage when a step-up load power from 500 to 1000 W is presented at the instant of 0.3 s. The transient process lasts for 40 ms and the average output voltage is regulated back to its reference of 300 V due to the integral effect of MFC method. The measured disturbance and its estimation of voltage control system are compared in the bottom subplot of Fig. 10. Similarly, the presented F_1 is multiplied by the capacitance C as well as its estimation so that they have the same dimension relation with load current. It is noticed that the estimation value F_{1e} converges to the measured disturbance asymptotically. It can be explained by the asymptotic properties of the closed-loop system, which is governed by the loop gain (46), although the AE behaves in a nonasymptotic manner. As shown in Fig. 10, the absolute value of F_{1e} in steady state is a little larger than that of the measured disturbance. It is because that the AE takes non-ideal factors, e.g., power losses, into account in the closed-loop voltage control system. In addition, F_{1e} is free of double-line frequency ripple, which avoid the distortion of reference input current.

To better understand the ability of the proposed control method, it is compared with a linear active disturbance rejection control (LADRC) counterpart, in which F_1 is estimated via an ESO [36]

$$\begin{cases} \dot{v}_{\mathrm{dc}e} = F_{1e} + \alpha_1 I_m + l_1(v_{\mathrm{dc}} - v_{\mathrm{dc}e}) \\ \dot{F}_{1e} = l_2(v_{\mathrm{dc}} - v_{\mathrm{dc}e}) \end{cases} \tag{47}$$

where $v_{\mathrm{dc}e}$ is the estimation of v_{dc}. l_1 and l_2 are the gains which leads to an observer bandwidth of w_{ESO}. To ensure a fair comparison, w_{ESO} is designed to be 140.5 rad/s, which is same as that of AE in the voltage control system according to (24). By utilizing the actual output voltage, the active disturbance rejection control law for voltage regulation has the same form as (43). From the simulation results shown in Fig. 10, one can see that MFC and LADRC have almost the same disturbance estimation and voltage regulation performance.

B. Experimental Results

The proposed model-free controller is experimentally tested. A programmable ac source supplies the boost ac/dc converter, which is connected to a dc electronic load. Control algorithms are implemented based on dSPACE ds1007 platform. Signal samplings are synchronized with PWM and triggered at the middle point of the rising edge of input current.

In the experimental tests, the proposed and the conventional PI control methods are compared when they are applied to the voltage and current control systems. In our case studies, the disturbance in current control system is mainly caused by the periodic input voltage and is measurable, thus, an FF strategy could eliminate its impact [4]. In this case, the PI controller is released to tackle only the reference tracking task and good current quality can be obtained. Other advanced controllers, e.g., predictive current controller in [7], share the same idea to reject the influence of input voltage by using its measured value. Therefore, the PI current control with duty ratio FF is adopted as the benchmark method in the experimental tests. It results in a current control system with a positive phase margin of 44.8° at a crossover frequency of 3 kHz. In terms of voltage control system, the NF-based PI controller is implemented for the purpose of comparison as in literatures, e.g., [14]–[16]. The same NF (44) is implemented. Phase margin and corresponding crossover frequency of the system are designed to be 50° and 20 Hz, respectively. Parameters of the PI controllers are also given in Table II.

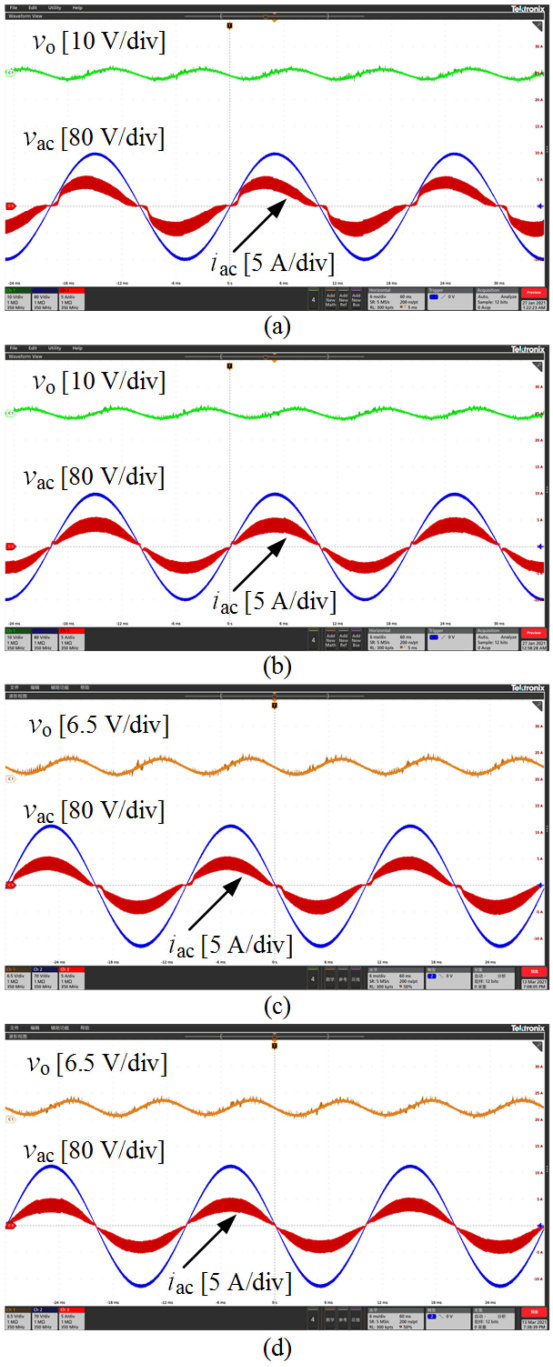

Fig. 11. Experimental results. Steady-state performance of the converter with load power of 300 W. (a) PI current control. (b) PI current control with duty ratio FF. (c) MFCC-II. (d) MFCC-I.

Fig. 11 compares the current tracking performance in steady state experimentally. As can be seen, the ac side input current is largely distorted with a sole PI controller. This is because the PI controller cannot handle well the reference tracking and disturbance rejection tasks simultaneously, especially when the system is affected by periodic disturbances. This problem is alleviated by integrating the duty ratio FF method, in which the effects of rectified input and output voltages are compensated. Better result is also observed with MFCC-II. One can see

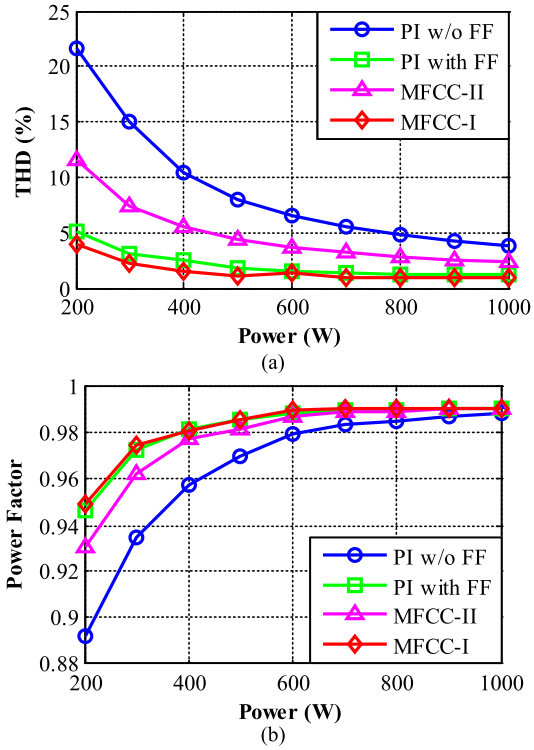

Fig. 12. Measured performance at the ac side of the converter under different load power. (a) THD of the ac side input current. (b) Power factor.

that a mere proportional tracking controller can get improved performance as long as the lumped disturbance is estimated and rejected via AE method. The performance can be further enhanced with MFCC-I as compared to MFCC-II. It is achieved due to higher loop gain at 100 Hz of MFCC-I as shown in Fig. 8.

The measured total harmonic distortion (THD) and power factor are presented in Fig. 12. It can be found that the PI controller with duty ratio FF achieves a good performance. It is because that the main disturbance caused by the periodic input voltage can be measured and compensated. The PI controller is released to tackle the reference tracking task only and the loop gain is properly shaped. In spite of this fact, comparison between MFCC-I and the PI controller with duty ratio FF demonstrates the superiority of the former. It indicates that the proposed MFC method can not only reject the known effects of the rectified input and output voltages, but also the unknown nonidealities of the converter, e.g., the parasitic resistance of the components.

Figs. 13 and 14 show the transient response of the converter under load variations with the NF-based PI control and the proposed MFC method, respectively. It can be observed that the PI control system has a sluggish dynamic response. In the first scenario, a negative load step change from 1000 to 500 W is tested. As shown in Fig. 13(a), the response time of PI control system is 115 ms and the overshoot of average output voltage is 12.5 V. In contrast, the output voltage of the converter with MFC recovers in 57 ms. The overshoot of its average value is reduced to 9.6 V. In case of load step-up change, it takes about 57 ms for the MFC system to recover from this transient process, which is only 46% of that of the PI control system. The undershoot

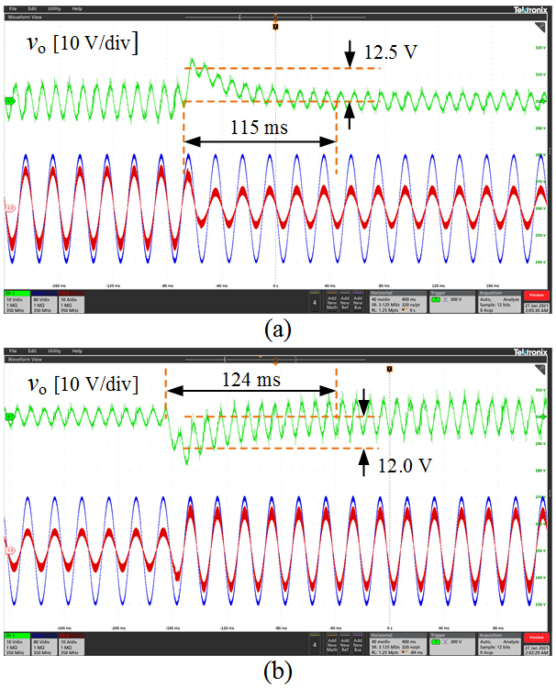

Fig. 13. Experimental results. Transient performance of the converter with PI control method. (a) Load step change from 1000 to 500 W. (b) Load step change from 500 to 1000 W.

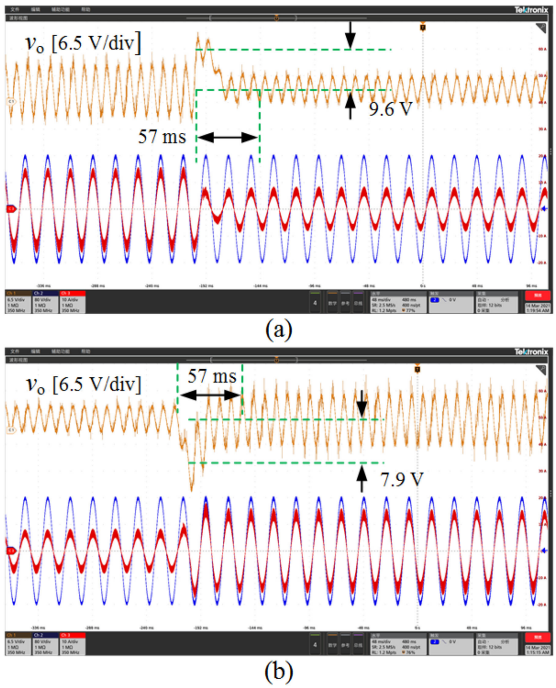

Fig. 14. Experimental results. Transient performance of the converter with MFC method. (a) Load step change from 1000 to 500 W. (b) Load step change from 500 to 1000 W.

of average output voltage is reduced from 12.0 to 7.9 V. The enhanced transient performance demonstrates the superiority of proposed MFC method of the converter. As compared to the PI control scheme, the load disturbance is estimated and compensated in real-time in the proposed control system via AE method. Thus, it shows good robustness against load variations. These results again indicate the disturbance rejection performance of MFC experimentally.

V. Conclusion

An MFC scheme is proposed in this article to improve the robustness against various disturbances for single-phase boost ac/dc converters. To form the theoretical basis, MFC theory is revisited via frequency domain analysis. AE, which plays an important role in MFC, can be characterized by a specially designed low-passing filter with unity gain and linear phase properties. It is demonstrated that the influence of uncertainties and disturbances can be eliminated by AEs within its passing band. Desired closed-loop output behavior can be achieved with a properly designed tracking controller and the AE. Model-free current and voltage control systems are designed in detail. Robustness of MFC against disturbances is verified experimentally. With the proposed control system, better current quality in steady state and enhanced transient voltage regulation is obtained.

References

[1] S. Li and C. Mi, "Wireless power transfer for electric vehicle applications," *IEEE J. Emerg. Sel. Topics Power Electron.*, vol. 3, no. 1, pp. 4–17, Mar. 2015.

[2] A. Khaligh and M. D'Antonio, "Global trends in high-power on-board chargers for electric vehicles," *IEEE Trans. Veh. Technol.*, vol. 68, no. 4, pp. 3306–3324, Apr. 2019.

[3] D. M. Van de Sype, K. De Gusseme, A. P. M. Van den Bossche, and J. A. Melkebeek, "Duty-ratio feedforward for digitally controlled boost PFC converters," *IEEE Trans. Ind. Electron.*, vol. 52, no. 1, pp. 108–115, Feb. 2005.

[4] K. P. Louganski and J.-S. Lai, "Current phase lead compensation in single-phase PFC boost converters with a reduced switching frequency to line frequency ratio," *IEEE Trans. Power Electron.*, vol. 22, no. 1, pp. 113–119, Jan. 2007.

[5] Y. Cho and J.-S. Lai, "Digital plug-in repetitive controller for single-phase bridgeless PFC converters," *IEEE Trans. Power Electron.*, vol. 28, no. 1, pp. 165–175, Jan. 2013.

[6] J.-H. Park, D.-J. Kim, and K.-B. Lee, "Predictive control algorithm including conduction-mode detection for PFC converter," *IEEE Trans. Ind. Electron.*, vol. 63, no. 9, pp. 5900–5911, Sep. 2016.

[7] H. S. Nair and N. L. Narasamma, "A computationally simple predictive CCM average current controller with nearly zero tracking error for boost PFC converter," *IEEE Trans. Ind. Appl.*, vol. 56, no. 5, pp. 5083–5094, Sep./Oct. 2020.

[8] A. Marcos-Pastor, E. Vidal-Idiarte, A. Cid-Pastor, and L. Martinez-Salamero, "Interleaved digital power factor correction based on the sliding-mode approach," *IEEE Trans. Power Electron.*, vol. 31, no. 6, pp. 4641–4653, Jun. 2016.

[9] N. Rathore, D. Fulwani, A. K. Rathore, and A. R. Gautam, "Adaptive sliding mode based loss-free resistor for power-factor correction application," *IEEE Trans. Ind. Appl.*, vol. 55, no. 4, pp. 4332–4343, Jul./Aug. 2019.

[10] A. Mallik, J. Lu, and A. Khaligh, "Sliding mode control of single-phase interleaved totem-pole PFC for electric vehicle onboard chargers," *IEEE Trans. Veh. Technol.*, vol. 67, no. 9, pp. 8100–8109, Sep. 2018.

[11] M. K. Ghartemani, S. A. Khajehoddin, P. K. Jain, and A. Bakhshai, "A systematic approach to DC-bus control design in single-phase grid-connected renewable converters," *IEEE Trans. Power. Electron.*, vol. 28, no. 7, pp. 3158–3266, Jul. 2013.

[12] Y. Levron, S. Canaday, and R. W. Erickson, "Bus voltage control with zero distortion and high bandwidth for single-phase solar inverters," *IEEE Trans. Power Electron.*, vol. 31, no. 1, pp. 258–269, Jan. 2016.

[13] S. A. Khajehoddin, M. Karimi-Ghartemani, P. K. Jain, and A. Bakhshai, "DC-bus design and control for a single-phase grid-connected renewable converter with a small energy storage component," *IEEE Trans. Power. Electron.*, vol. 28, no. 7, pp. 3245–3254, Jul. 2013.

[14] S. Taghizadeh, M. J. Hossain, J. W. Lu, and M. Karimi-Ghartemani, "An enhanced DC-bus voltage control loop for single-phase grid-connected DC/AC converters," *IEEE Trans. Power. Electron.*, vol. 34, no. 6, pp. 5819–5829, Jun. 2019.
[15] S. Taghizadeh, M. Karimi-Ghartemani, M. J. Hossain, and J. Lu, "A fast and robust DC-bus voltage control method for single-phase voltage-source DC/AC converters," *IEEE Trans. Power Electron.*, vol. 34, no. 9, pp. 9202–9212, Sep. 2019.
[16] S. Li, W. Lu, S. Yan, and Z. Zhao, "Improving dynamic performance of boost PFC converter using current-harmonic feedforward compensation in synchronous reference frame," *IEEE Trans. Ind. Electron.*, vol. 67, no. 6, pp. 4857–4866, Jun. 2020.
[17] M. Merai, M. W. Naouar, I. Slama-Belkhodja, and E. Monmasson, "An adaptive PI controller design for DC-link voltage control of single-phase grid-connected converters," *IEEE Trans. Ind. Electron.*, vol. 66, no. 8, pp. 6241–6249, Aug. 2019.
[18] J. Honkanen, J. Hannonen, J. Korhonen, N. Nevaranta, and P. Silventoinen, "Nonlinear PI-control approach for improving the DC-link voltage control performance of a power-factor-corrected system," *IEEE Trans. Ind. Electron.*, vol. 66, no. 7, pp. 5456–5464, Jul. 2019.
[19] P.-A. Gedouin, E. Delaleau, J.-M. Bourgeot, C. Join, S. A. Chirani, and S. Calloch, "Experimental comparison of classical PID and model-free control: Position control of a shape memory alloy active spring," *Control Eng. Pract.*, vol. 19, no. 5, pp. 433–441, May 2011.
[20] L. Menhour, B. d'Andrea-Novel, M. Fliess, D. Gruyer, and H. Mounier, "An efficient model-free setting for longitudinal and lateral vehicle control: Validation through the interconnected pro-SiVIC/RTMaps prototyping platform," *IEEE Trans. Intell. Transport. Syst.*, vol. 19, no. 2, pp. 461–475, Feb. 2018.
[21] Y. Zhou, H. Li, R. Liu, and J. Mao, "Continuous voltage vector model-free predictive current control of surface mounted permanent magnet synchronous motor," *IEEE Trans. Energy Convers.*, vol. 34, no. 2, pp. 899–908, Jun. 2019.
[22] Y. Zhang, T. Jiang, and J. Jiao, "Model-free predictive current control of DFIG based on an extended state observer under unbalanced and distorted grid," *IEEE Trans. Power Electron.*, vol. 35, no. 8, pp. 8130–8139, Aug. 2020.
[23] B. Park and M. M. Olama, "A model-free voltage control approach to mitigate motor stalling and FIDVR for smart grids," *IEEE Trans. Smart Grid*, vol. 12, no. 1, pp. 67–78, Jan. 2021.
[24] H. Abouaissa and S. Chouraqui, "On the control of robot manipulator: A model-free approach," *J. Comput. Sci.*, vol. 31, pp. 6–16, Feb. 2019.
[25] J. Sun, J. Wang, P. Yang, Y. Zhang, and L. Chen, "Adaptive finite time control for wearable exoskeletons based on ultra-local model and radial basis function neural network,," *Int. J. Control Automat. Syst.*, vol. 19, no. 2, pp. 889–899, Feb. 2021.
[26] G. P. Neves and B. A. Angelico, "Model-free control of mechatronic systems based on algebraic estimation," *Asian J. Control*, to be published, doi: 10.1002/asjc.2596.
[27] M. Fliess and C. Join, "Model-free control," *Int. J. Control*, vol. 86, no. 12, pp. 2228–2252, 2013.
[28] Y. Zhang, J. Jin, and L. Huang, "Model-free predictive current control of PMSM drives based on extended state observer using ultralocal model," *IEEE Trans. Ind. Electron.*, vol. 68, no. 2, pp. 993–1003, Feb. 2021.
[29] M. Fliess and H. Sira-Ramirez, "An algebraic framework for linear identification," *ESAIM, Control Optim. Calculus Variations*, vol. 9, no. 9, pp. 151–168, 2003.
[30] M. Mboup and S. Riachy, "Frequency-domain analysis and tuning of the algebraic differentiator," *Int. J. Control*, vol. 91, no. 9, pp. 2073–2081, Sep. 2018.
[31] F. Beltran-Carbajal and G. Silva-Navarro, "A fast parametric estimation approach of signals with multiple frequency harmonics," *Elect. Power Syst. Res.*, vol. 144, pp. 157–162, Mar. 2017.
[32] A. Gensior, J. Weber, J. Rudolph, and H. Guldner, "Algebraic parameter identification and asymptotic estimation of the load of a boost converter," *IEEE Trans. Ind. Electron.*, vol. 55, no. 9, pp. 3352–3360, Sep. 2008.
[33] H. Yuan, S. Li, S. C. Tan, and S. Y. R. Hui, "Sensor count reduction for single-phase converters with an active power buffer using algebraic observers," *IEEE Trans. Ind. Electron.*, vol. 68, no. 11, pp. 10666–10676, Nov. 2021.
[34] H. Yuan, S. Li, S. C. Tan, and S. Y. R. Hui, "Simplified algebraic estimation technique for sensor count reduction in single-phase converters with an active power buffer," *IEEE Trans. Power Electron.*, vol. 36, no. 10, pp. 11444–11455, Oct. 2021.
[35] T. V. Tran, K.-H. Kim, and J.-S. Lai, "Optimized active disturbance rejection control with resonant extended state observer for grid voltage sensorless LCL-Filtered inverter," *IEEE Trans. Power Electron.*, vol. 36, no. 11, pp. 13317–13331, Nov. 2021.
[36] G. Herbst, "Practical active disturbance rejection control: Bumpless transfer, rate limitation, and incremental algorithm," *IEEE Trans. Ind. Electron.*, vol. 63, no. 3, pp. 1754–1762, Mar. 2016.

Hengguo Zhang was born in Anhui, China, in 1992. He received the B.S. degree in electrical engineering in 2013, from the Hefei University of Technology, Hefei, China, where he is currently working toward the Ph.D. degree in electrical engineering.

His research interests include linear system theory, design and control of power converters.

Hongmei Li was born in Anhui, China, in 1969. She received the B.S. and M.S. degrees in electrical engineering from the Hefei University of Technology, Hefei, China, in 1991 and 1996, respectively, and the Ph.D. degree in electrical engineering from Shenyang University of Technology, Shenyang, China, in 2003.

She has been a Professor with the Department of Electrical Engineering, Hefei University of Technology, since 2006. From 2004 to 2005, she has been with Hikihara Laboratory, Kyoto University, Kyoto, Japan, as a Visiting Scholar. In 2012, she has been with the Center for Automotive Research, The Ohio State University, Columbus, ON, USA, as a Visiting Scholar. Her research interests include power electronics and motor control, fault diagnosis, and fault-tolerant control of electrical machine systems.

Jingkui Mao was born in Henan, China, in 1978. He received the B.S. degree in automation from the Central South University of Technology, Changsha, China, in 2002. He is currently working toward the Ph.D. degree with the Department of Electrical Engineering and Automation, Hefei University of Technology, Hefei, China.

He is currently an Associate Professor with Henan institute of technology, Henan, China. His research interests include the predictive control and discrete space vector pulse modulation of electrical motor drives.

Chen Pan was born in Wuhu, China, in 1997. He received the B.S. degree in electrical engineering in 2019 from the Hefei University of Technology, Hefei, China, where he is currently working toward the M.S. degree in electrical engineering.

His research interests include advanced control strategy of single-phase boost ac/dc converters.

Zhiyuan Luan was born in Anhui, China, in 1996. He received the B.S. degree in electrical engineering in 2017 from the Hefei University of Technology, Hefei, China, where he is currently working toward the M.S. degree in electrical engineering.

His research interests include the design and control of high-frequency switching power converters.